In situ scanning electron microscopy indentation studies on multilayer nitride films: Methodology and deformation mechanisms

K.A. Rzepiejewska-Malyska[a)]
EMPA, Materials Science and Technology—Laboratory for Mechanics of Materials and Nanostructures, Thun CH-3602, Switzerland

W.M. Mook
EMPA, Materials Science and Technology—Laboratory for Mechanics of Materials and Nanostructures, Thun, BE Switzerland

M. Parlinksa-Wojtan
EMPA, Materials Science and Technology—Nanoscale Materials Science, Dübendorf, ZH Switzerland

J. Hejduk
Polish Academy of Sciences—Institute of Electron Technology, Warsaw 02-668, Poland

J. Michler
EMPA, Materials Science and Technology—Laboratory for Mechanics of Materials and Nanostructures, Thun, BE Switzerland

(Received 31 July 2008; accepted 5 December 2008)

Systematic studies of the deformation mechanisms of multilayer transition metal nitride coatings TiN/CrN, TiN/NbN, and NbN/CrN, and corresponding reference coatings of TiN, NbN, and CrN deposited by a direct current (dc) magnetron sputtering process onto silicon ⟨100⟩ have been performed. Mechanical characterization was conducted using a combination of microindentation and nanoindentation in the load range 30 to 150 mN and 0.5 to 3.5 mN, respectively. For both load ranges, scanning electron microscopy (SEM) in situ indentation was used to observe the indentation process including any pileup, sink-in, and fracture mechanisms specific to each coating. The coatings' microstructure, both before and after indentation, was analyzed using transmission electron microscopy (TEM). It was possible to both correlate the indentation load–displacement response to surface roughness effects and fracture modes (substrate and film cracking) and observe deformation mechanisms within the coatings.

I. INTRODUCTION

Transition metal nitride coatings have traditionally been used as protective coatings for different types of cutting tools and microelectronics and as diffusion barriers for the semiconductor industry, and they are now being considered for use as protective coatings in microelectromechanical systems (MEMS).[1,2] This is due to their high hardness and reasonable toughness, which combine to give superior tribological performance compared to uncoated devices.[3–5] Tribological issues are especially important for MEMS applications where excessive wear of the single- and polycrystalline silicon elements in motion drastically limit device designs and lifetimes.

The most extensively explored transition metal nitride coatings are TiN, CrN, NbN, TaN, VN, and ZrN.[1,2,6] This work focuses on three of these, namely TiN, CrN, and NbN, because of their outstanding mechanical properties. All of these transition metal nitrides are relatively hard with values ranging from 21 to 25 GPa for TiN,[7–9] from 14 to 22 GPa for CrN[10,11] and from 6 to 45 GPa for NbN,[12–14] depending on the deposition technique and its conditions. Moreover, all of these materials are reported to have good wear resistance[6,14,15] and fracture toughness.[1,16]

These materials also possess some individual properties that differentiate them from each other. Both CrN and NbN have good oxidation and corrosion resistance,[17,18] contrary to TiN. On the other hand, TiN is biocompatible,[19,20] can act as a good diffusion barrier,[21,22] and exhibits interesting optical properties.[18] NbN and TiN both have high melting points,[14] and NbN shows high electrical conductivity.[23,24] Thus, NbN was first developed for a variety of applications such as superconducting electronics,[25] field-emission cathodes,[26] and microelectronics. Such interesting combinations of properties have brought these nitrides under continuous development since mid-1980s,[18,25] not only for tribological applications[3,27] but also for decorative

[a)]Address all correspondence to this author.
e-mail: Karolina.Rzepiejewska@empa.ch
DOI: 10.1557/JMR.2009.0139

applications in the case of TiN.[28] It is thought that if these constituent materials could be properly combined, for example as multilayer nanolaminates, their combined properties could be tailored for specific applications.

Multilayer coatings are reported to have enhanced resistance to wear, cracking, and fracture when compared with single-layered structures.[8,29] This is true for both epitaxial superlattice structures[8] and polycrystalline multilayer thin films[30]; however, enhancement mechanisms for these two laminate structures differ because of microstructural differences. The hardness increase of single-crystal nanolaminates is generally attributed to the superlattice effect[31,32] while a rule-of-mixture argument is used for polycrystalline coatings.[29,30,33] Any increase beyond the rule-of-mixture value for polycrystalline nanolaminates is often explained by the modified Hall–Petch theory.[34,35] The improved fracture toughness of the multilayer coatings compared with the single-layer coatings can be explained by crack deflection at the interlayer interfaces.[36] Moreover, any dislocation multiplication in adjacent layers is hampered by the layer interfaces that can act as grain boundaries.[37]

A full understanding of the deformation and fracture mechanisms of multilayer coatings has been hindered by their complexity.[38] Depending on the constituent materials in the multilayer coating, polycrystalline nanolaminate structures are reported to deform by different mechanisms. The most commonly observed are grain-boundary sliding for TiN/NbN and TiN/(Ti,Al)N[31,39] and densification underneath the indentation imprint for TiN/NbN.[40,41]

Hard materials, such as transition metal nitrides and their multilayer combinations, are generally characterized by their hardness, H, reduced modulus, E_r, and elastic recovery, W_e. These quantities can be determined from load–displacement curves obtained by instrumented indentation.[42] However, a number of assumptions concerning the material behavior must be made when analyzing indentation data. Most models are based on the indentation of a flat, elastic half-space and the assumption that the tip area function (calculated by indenting a reference material) is applicable to other, similar materials. Mechanical properties such as nanohardness and reduced modulus have been widely studied for a number of different nitride multilayer systems. The most extensively tested among others are TiN/CrN[11,32] and TiN/NbN[41,43] and more complex combinations containing CrN such as TiN–CrAlN and CrN–CrAlN.[44,45]

However as shown in Sec. III. D, even the same class of materials (in this case metal nitrides) can behave differently at both the micro- and nanoscales with regard to material pileup and sink-in around the tip during an indentation. These types of behaviors can greatly affect both the calculated hardness and modulus values and are not apparent by observing only the load–displacement response. On the other hand, thin-film fracture is generally seen in instrumented indentation as a pop-in.[46] However, this may also be misleading as it is shown in Sec. III. D. 1 that crack initiation is not always associated with pop-in events.

These issues can be addressed by in situ indentation performed inside a scanning electron microscope (SEM) since this technique allows for the pileup, sink-in crack initiation and propagation and shear band formation[47] to be observed at the scale of interest in real time. This provides additional information on fracture toughness and strain hardening behavior that facilitates proper quantitative data evaluation, enabling a more accurate calculation of contact area and an improved mechanical model.[48] This information, when combined with post-mortem transmission electron microscopy (TEM) studies of the film cross sections beneath the indents, increases understanding of the underlying deformation mechanisms of the studied coatings.

Our previous work was focused on in situ SEM microindentation studies of TiN, CrN, and their multilayer combinations.[49] In this paper, three multilayer coatings, namely TiN/CrN, NbN/CrN, and TiN/NbN, with individual layer thickness of approximately 17 nm, consisting of 20 periods in total, were systematically investigated by both in situ SEM micro- and nanoindentation. For comparison, single-layer reference coatings of TiN, CrN, and NbN were deposited at least as thick as their multilayer counterparts. In situ SEM microindentation was used to investigate the presence of pileup and sink-in, as well as cracking behavior at the microscale for all of the deposited film/substrate combinations. This large-scale indentation was complemented by in situ high-resolution SEM nanoindentation, which provided information about nanomechanical behavior for depths not exceeding the 15% of the total coating thickness. Cross sections of the residual indent impressions were created by focused ion beam (FIB) milling and analyzed using TEM so that the type of microstructure, as well as deformation mechanisms within the films, could be characterized. The average chemical composition of the thick reference coatings was assessed with glow discharge optical emission spectroscopy (GDOES).

II. EXPERIMENTAL DETAILS

Transition nitride multilayer thin films were deposited with ultrahigh vacuum (UHV) direct current (dc) magnetron sputtering in a Leybold L400Sp system on ⟨100⟩-oriented silicon substrates at a substrate temperature of ~70 °C.[50,51] Three different types of multilayer combinations, namely TiN/NbN, NbN/CrN, and TiN/CrN[49] and corresponding single-layer reference coatings of TiN, NbN, and CrN were deposited (see Table I).[45,49]

Hardness and Young's modulus values of the coatings were obtained by nanoindentation using a TriboIndenter (Hysitron, Inc., Minneapolis, MN) equipped with a Berkovich-shape diamond tip. This indenter tip geometry

TABLE I. Basic information about investigated films.

Type of coating	Materials	Range of column width (nm)	Average composition (at.%)		Average thicknesses of the layers in the coating (nm)	Measured thickness of the coating (nm)	Compression (%)
			X	N			
Reference	TiN	~10–30	35	65	···	646	~4
	CrN	~150	85	15	···	1069	~11
	NbN	~15	55	45	···	780	~3.8
Multilayers	TiN/NbN	~30–60	···	···	16.66/16.28	659	~19.5
	TiN/CrN	~50	···	···	18.03/17.52	697	~20.4
	NbN/CrN	~15–200	···	···	19.61/18.65	765	~16.5

Column widths and thicknesses were determined by TEM, composition was measured with GDOES, and the compression (%) is the decrease in film thickness below 30 mN indents. (*X* = Ti, Cr, Nb).

allows for indentation while applying relatively low strain gradients, which decreases the probability of sample cracking. The penetration depth was limited to the range of 5 to 15% of the total coating thickness to minimize errors associated with surface effects (the lower limit) and the influence of the substrate (the upper limit).[52] The coating surface influence can have its source in many different principles. Too low of an indentation depth may result in unnaturally high hardness caused by unfavorable ratios of surfaces roughness to tip radius of curvature and surface roughness to indentation depth.[53] To stay within the optimal displacement regime, the applied load ranged from 0.5 to 3.5 mN. The indenter was operated in the open-loop loading mode with loading and unloading portions of 5 s each. Therefore, the average load rate varied depending on the maximum load, namely 0.1 mN/s for 0.5 mN, 0.2 mN/s for 1 mN, 0.5 mN/s for 2.5 mN, and 0.7 mN/s for 3.5 mN. These loading rates did not influence the measured hardness or reduced modulus. To ensure accurate data estimation, values presented in this work are averages of at least eight measurements, while the error bars represent three standard deviations that correspond to the range containing 99.97% of possible values.[54]

To investigate the incipient stages of deformation at displacements of less than 15% of the coating thickness, a Hysitron PicoIndenter (Hysitron, Inc.) integrated into high-resolution SEM (Hitachi S-4800, Japan) was used.[55]

Indentation experiments were also performed at the microscale with the in situ microindenter developed and integrated into a Zeiss DSM962 SEM (Germany) by Rabe et al.[48] For these experiments, a cube corner indenter tip was used. The load-controlled indentation experiment with a maximum load of 150 mN was performed on all investigated samples. The indentation experiment consists of 60 s of linear loading, a hold segment at maximum load, and unloading segment, 30 s long each. Therefore, the average loading and unloading rate were equal to 2.5 and 5 mN/s, respectively. Such a high load was necessary to reach the onset of crack formation and failure modes characteristic for each type of coating. As the depth of indentation far exceeded 15% of the coating thickness for these experiments, the mechanical behavior of the coating–substrate system was probed.

TEM foils were prepared in a way that the coatings' microstructure and deformation mechanisms could be characterized. Foils of the cross sections of the as-deposited coatings and of the residual plastic impressions from 30 mN indents were prepared using a FIB-Dual Beam FEI STRATA DB235 external lift-out technique (FEI, The Netherlands). Transmission electron microscopy in both bright field (BF) and dark field (DF) were performed on a CM30 Philips LaB6 TEM (FEI) using 300 kV acceleration voltage, reaching a point resolution of 2.6 Å.

III. RESULTS AND DISCUSSION

A. Microstructure of the investigated thin films

Dark-field micrograph analysis allowed for comparison of the microstructure for all coatings. As can be seen for both reference and multilayer coatings, the structure is generally nanocrystalline with randomly oriented grains as seen in Fig. 1. Reference coatings show columnar growth with increasing grain size toward the film surface. The average column width varies between 15 nm for NbN and 150 nm for CrN,[56] as summarized in Table I. Both CrN and TiN have columns extending through the entire film thickness, but TiN shows high-angle boundaries whereas CrN has low-angle boundaries columns. NbN grains exhibit a subgranular structure with many differently oriented zones. A nucleation zone with an unresolved nature (amorphous or nanocrystalline) was observed close to the substrate/film interface.

From the TEM micrographs in Fig. 1, the constituent layers in the multilayer coatings interacted differently in each pair during deposition. The NbN/CrN multilayers show smooth layers with sharp and smooth interfaces in the BF image. However, columnar grains grow within multilayered structure having a sublayer structure. In the DF image, the CrN–NbN interface in the direction of deposition is very sharp, contrasting with the NbN–CrN interface. This may occur because the NbN has high-angle boundaries unlike CrN, which has low-angle boundaries. The TiN/CrN is characterized by flat layers

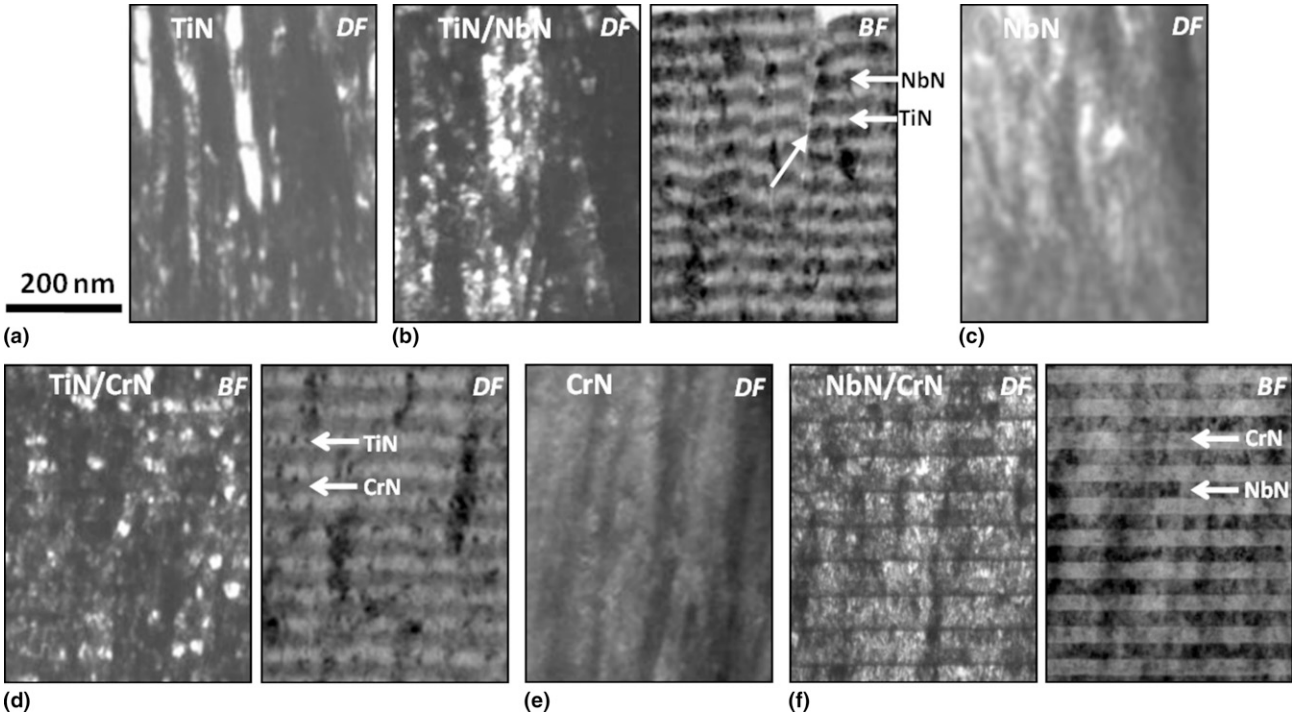

FIG. 1. TEM cross-sectional analysis for as-deposited coatings with dark field (DF) for all coatings in addition to bright field (BF) for multilayers. (a) TiN showing high levels of misorientation. (b) TiN/NbN showing columnar grain growth through layers. (c) NbN exhibiting granular structure with subgranular misorientation. (d) TiN/CrN showing multilayer grain orientation. (e) CrN showing large columnar grains. (f) NbN/CrN with crisp interfaces.

and interfaces of higher roughness compared with NbN/CrN. This combination[49] exhibits a granular microstructure such that the columns can grow through several layers.[30] TiN/NbN has nonflat layers with rough and wavy interfaces, which is probably caused by the competitive growth of strongly misoriented columnar grains. For the TiN/NbN combination, the grain boundaries are visible as white vertical lines [see Fig. 1(b), arrow]. Voids occurred as a result of kinetic limitations of the deposition process that separate the columnar grains. In the TiN constituent layers for both TiN/NbN and TiN/CrN combinations, small grains of TiN are nested between larger columnar grains, and therefore the presence of the layered structure confines the TiN microstructure.

B. Chemical composition of reference coatings

The chemical composition of the reference coatings was assessed using the GDOES technique. The use of thick coatings allows for more accurate data interpretation. The as-deposited materials are nonstoichiometric to varying degrees as is summarized in Table I. Following that, the TiN composition is very rich in N (~65 at.%), while CrN contains only 15% N (see Table I).[16] The NbN is close to stoichiometric composition, which is in agreement with previous studies.[57] The concentration of each constituent element is constant through the film thickness. Relatively low deposition temperatures (substrate temperature during deposition ~70 °C)[50] implies that the deposition is not thermodynamically stable and suggests that the coatings contain a mixture of different phases.[58] Chemical composition was studied extensively for each of the binary combinations and is reported for Ti–N,[58–60] for Nb–N,[61,62] and for Cr–N.[63,64]

C. Ex-situ nanoindentation

Film systems were indented with a Hysitron TriboIndenter with loads ranging from 0.5 to 3.5 mN to quantify hardness and reduced modulus without substrate influence. These results can be seen in Fig. 2. The NbN reference coating shows much higher hardness and reduced modulus when compared with the other coatings. Hardness increases in this case with increasing indentation depth, from 20.4 to 32.7 GPa, while reduced modulus maintains a value between 276 and 287 GPa throughout the range of applied loads. All of the other reference and multilayer films had hardnesses in the range of 10 to 20 GPa, while reduced moduli ranged from 180 to 240 GPa. Within the measurement accuracy, the two nanolaminates that contain the NbN do not follow the rule of mixture either for hardness or for modulus. The values decrease to the other constituent material properties; the reason for which is explained in Sec. III. D. 2. As is shown with ex situ nanoindentation alone, it is impossible to determine why the hardness and

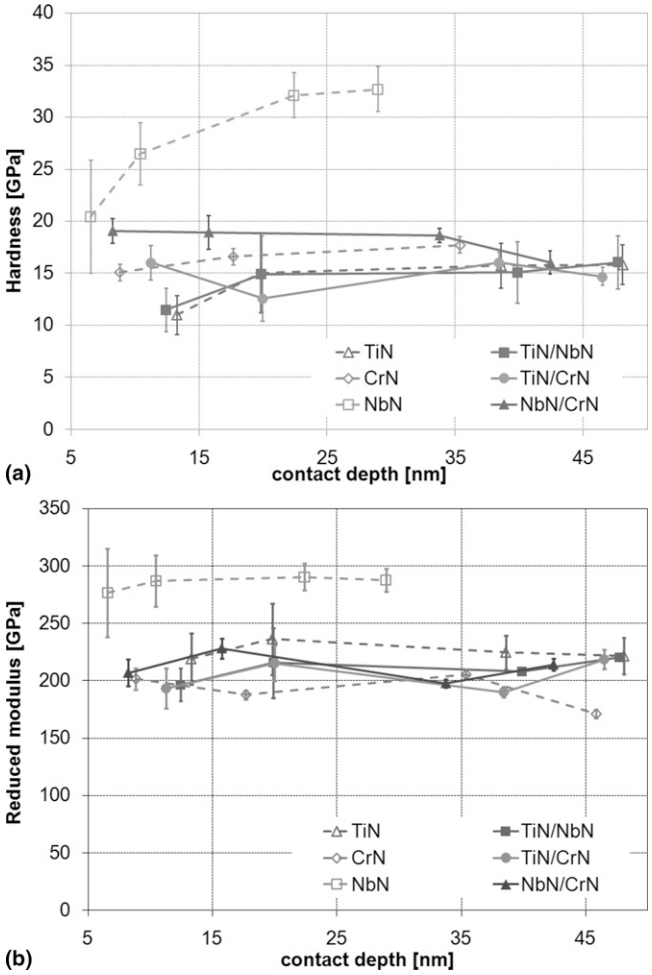

FIG. 2. Hardness (a) and reduced modulus (b) as a function of the contact depth for all coatings from ex situ nanoindentation determined using the Oliver and Pharr approach.

reduced modulus values are practically the same for all the coatings even though they are made from different materials. For further insight, the in situ SEM indentation at both the micro- and nanoscale was performed.

D. In situ SEM micro/nanoindentation

The main goal for the in situ investigation was to correlate any cracking and spalling that may be observed during indentation as seen in Figs. 3 and 6 with events that occurred on the corresponding load–displacement curves in Figs. 5 and 8 such as pop-ins or other discontinuities. The in situ indentation performed at the microscale allowed for fracture mechanism observations, while indentation at the nanoscale concentrated on pileup and sink-in of the films independently on the substrate influence.

1. In situ SEM microindentation

During in situ SEM microindentation, movies can be recorded throughout the indentation process. Indentations to a maximum load of 150 mN were conducted, and the residual impressions from these indentations are compiled in Fig. 3. The load–displacement response from these are shown in Fig. 5, where an indentation into the bare Si is repeated in each figure as an aid when comparing coating performance. Figures 5(a)–5(c) show multilayers and corresponding reference coatings responses. Figure 5(d) shows the load–displacement curves for reference coatings for comparison. All films show cracking in Fig. 3 except for the NbN reference film, which spalled off during the first part of unloading [the inset of Fig. 3(c′) shows the film at maximum load without cracking]. In this case, the spalling could be caused by either weak coating–substrate adhesion or high residual stress that can be superimposed on the contact stress. The spalled coating reveals the damage that occurred in the substrate in the form of lateral cracking, but it does not show up in the load–displacement curve in the form of a discontinuity [Fig. 5(d)]. For all of the other coatings, the initiation and growth of the radial cracks can be correlated to the load–displacement response by isolating individual in situ movie frames. For example, the initiation and growth of cracks in the CrN reference film can be seen in Fig. 4 where it is immediately apparent that there is not an excursion (in load or displacement) that corresponds to the visible cracking. This is true for the other specimens as well where the indentation depth and load for crack initiation along with the crack length at maximum load are compiled in Table II. These cracks are nucleated in the coatings during the loading portion of the indentation experiment and grow slowly and continuously until the maximum load is reached. Subsequently, they open more or even grow in during the unloading part of the test. Finally, they close again as the tip loses contact with the surface. The exact moment of the tip–material relative motion is visible on the load–displacement curves by a regular kink during unloading, marked out by the circle on Fig. 5(b).

In these films, the process of cracking is not rapid and does not provide quick energy release. The radial cracks within the coating are most likely the consequence of lateral cracking beneath the coating within the substrate similar to what is observed in Fig. 3(c). The repeating pop-ins present at ~30 mN further suggest that internal, nonvisible cracks occurred in this structure before appearing on the coating surface [Fig. 5(b), circle]. Substrate cracking enhances the local tensile strain within the coating, which contributes to the cracking. A pop-in was observed on the load–displacement curve only for TiN/NbN, albeit at a lower load than the surface crack was nucleated [Fig. 5(b), arrow]. Although these coatings happen to crack at high loads, they provide a significant improvement over the response of the bare Si substrate, which revealed many well-pronounced

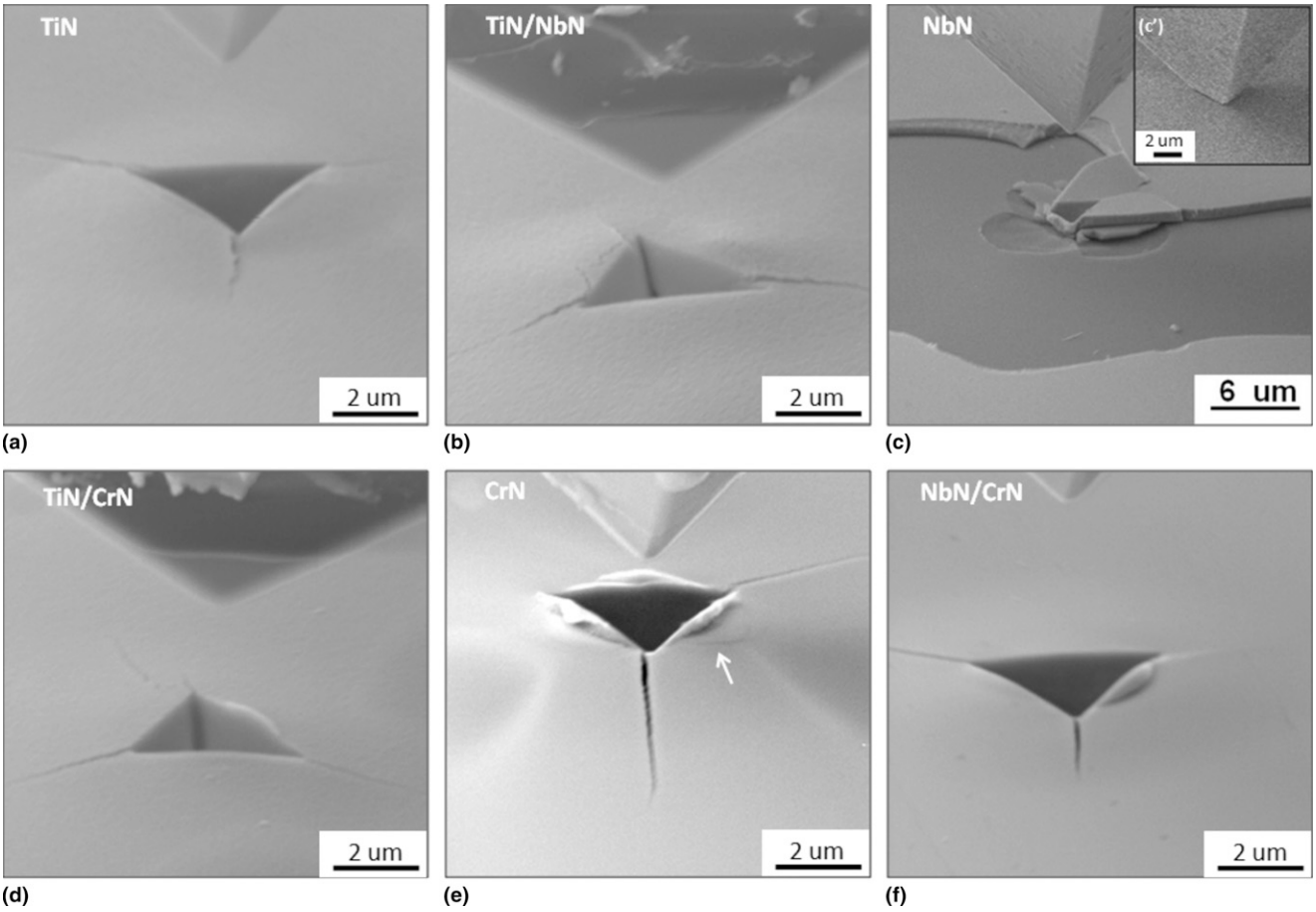

FIG. 3. In situ SEM nanoindentation images of the indentation imprints for a maximum load of 150 mN on the following coatings: (a) TiN, (b) TiN/NbN, (c) remnants of NbN coating, (c′) complete NbN coating under maximum load, (d) TiN/CrN, (e) CrN, and (f) NbN/CrN.

pop-ins that did not happen for the coated substrates as seen in Fig. 5.

2. In situ SEM nanoindentation

In situ high-resolution SEM nanoindentation was performed using a Hysitron PicoIndenter.[55] Applying a maximum load of ~900 μN, which is close to the limit for this type of sensor, the deformation mechanisms of the coatings were studied independently from the influence of the substrate. Residual impressions from these indents can be seen in Fig. 6, while the corresponding load–displacement curves can be seen in Fig. 8. Roughnesses of these coatings vary and influence the initial stiffness during the indentation. This is clearly seen for NbN/CrN in Fig. 8 where the load increases at once, unlike the TiN/NbN coating.

The deformation modes observed in situ during nanoindentation are consistent with the information available from the load–displacement curves. Indentation curves for CrN show significant plasticity, while NbN has greater elastic deformation [Fig. 8(d)]. The presence of TiN in the TiN/NbN multilayer coating determined the amount of the plasticity present during deformation [Fig. 8(b)].

Hardness values from the in situ SEM nanoindentation experiment were calculated using the contact area at maximum load determined from the in situ movies along the maximum load from the data in Fig. 8. These values, listed in Table III, depend on the SEM image resolution and are therefore subject to a small amount of error. They are compared with hardness values obtained using the Oliver and Pharr[65] method from 1000 μN indents obtained with a Hysitron TriboIndenter instrument. All of the coatings that contain NbN indicate that in situ SEM hardness values are higher than those obtained by the Oliver and Pharr method. For these coatings, a large amount of sink-in are visible during the experiment (see e.g., Fig. 7). Such phenomena as pileup and sink-in were not taken into account in the ex situ experiments. Therefore, the apparent contact area was overestimated, thus lowering both the hardness and reduced modulus. When accounting for the sink-in from the in situ indentations, hardness of the TiN/NbN multilayer increases to 19 GPa, while the NbN/CrN increases to more than 37 GPa. That is a 100% increase in calculated hardness when compared with the ex situ values calculated using the Oliver and Pharr method.

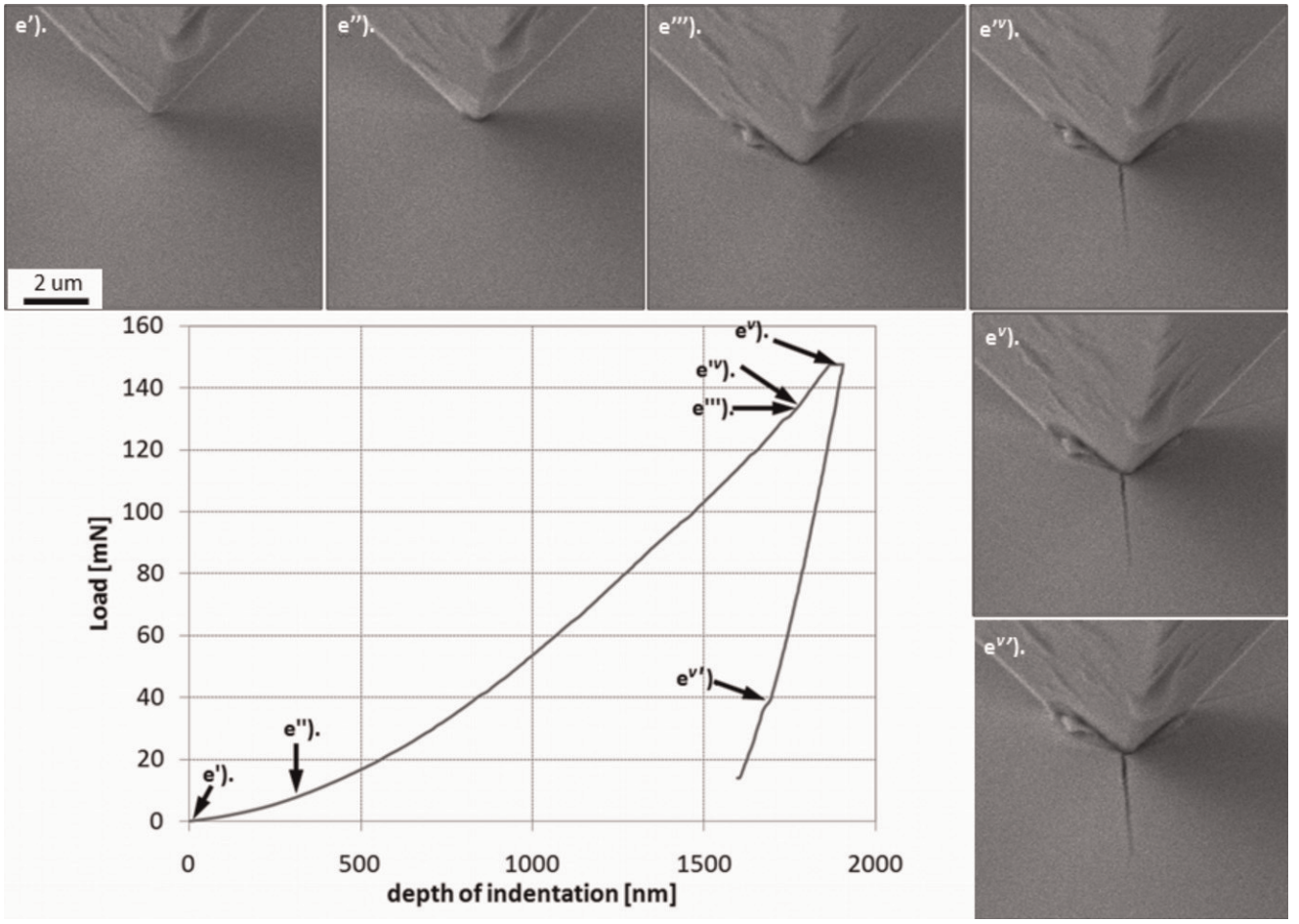

FIG. 4. Frames of indentation [see Fig. 3(e)] showing the different stages of deformation of the CrN reference coating and corresponding load–displacement curve. (e′) First contact of the indenter tip with the coating surface area. (e″) First moment of pileup formation. (e‴) The moment of piling up of the coating just before the crack formation. (e'^{v}) First moment of cracking (crack appeared very rapidly). (e^{v}) Coating under the maximum load. ($e^{v\prime}$) The moment of tip form the coating reliving.

On the other hand, the materials that pile up demonstrate a decrease in the measured hardness (note that the contact between indenter tip and the CrN was obscured so an in situ hardness value could not be accurately determined for that case). For example, the TiN/CrN multilayer exhibits a decrease in calculated hardness from 14.9 to 10.5 GPa. Interestingly for the NbN/CrN coating, where the reference films show dissimilar behaviors (sink-in for NbN and pileup for CrN), sink-in is observed generating a hardness level equal to that of the NbN reference coating at the nanoscale.

E. TEM analysis of the deformed area

Cross-sectional TEM analysis of the plastic deformation beneath 30 mN indents was conducted on both multilayers and reference coatings; the resulting images are shown in Fig. 9. From this, it can be seen that the TiN reference coating [Fig. 9(a)] deforms through cracks [Fig. 9(a′), arrow] and shears along the columnar boundaries, which result in formation of steps at the coating/substrate interface [Fig. 9(a″)]. This was also found in previous studies.[38,49] Additionally, deformation and delamination in the form of buckling, characteristic for hard coatings on a softer substrate[66] appeared at the coating/substrate interface. The CrN reference film [Fig. 9(e)] densifies, which is also consistent with previous studies.[66] However, CrN was also subject to material flow, which occurred in the form of pileups along the indentation imprint edges and formation of shear bands visible in Fig. 3(e). The last among the reference coatings, NbN [Fig. 9(c)] behaves like an elastic plate, and the majority of the plastic deformation is confined within the substrate. The smallest amount of permanent deformation is observed for NbN and TiN reference coatings, 3.8% and 4%, respectively, while for CrN it is ~11% (see Table I). These values are the percent decrease in coating thickness underneath the indent. This deformation is a combination of changes in material volume caused by material porosity that may

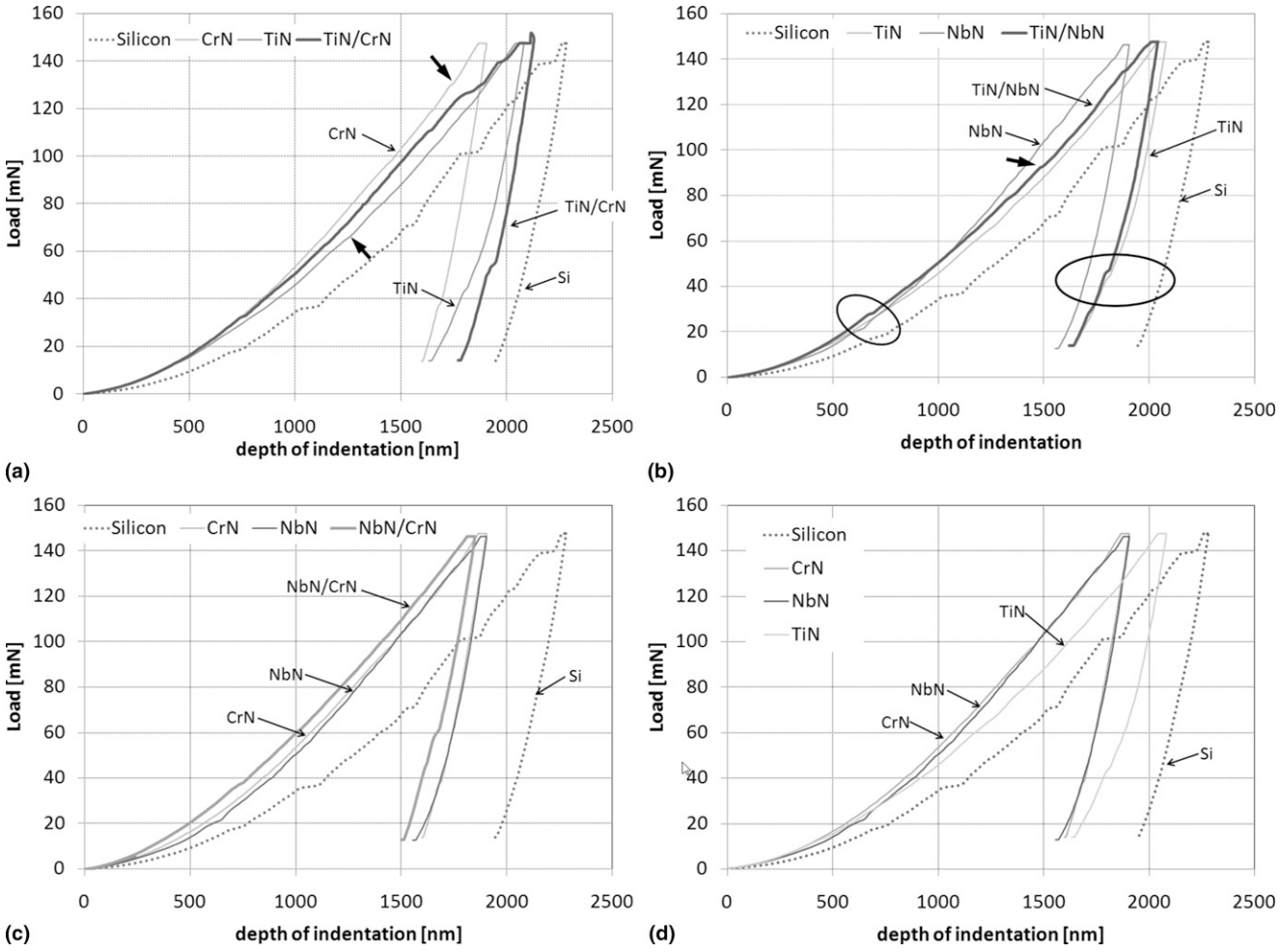

FIG. 5. Load–displacement curves of the multilayers and corresponding reference coatings that were recorded during in situ SEM microindentation (see Fig. 3). (a) TiN/CrN, CrN, and TiN. (b) TiN/NbN, NbN, and TiN. (c) NbN/CrN, NbN, and CrN. (d) TiN, CrN, and NbN.

not be visible on the TEM micrographs, flattening of the rough coating surface, and dislocation-mediated plastic flow.

For the TiN/CrN [Fig. 9(d″)] and NbN/CrN [Fig. 9(f′)] coatings, indentation caused multilayer structural rotation similar to previous studies of polycrystalline[39] and single-crystal coatings.[67] Grain rotation is observed to be ∼10° for TiN/CrN and ∼15° for NbN/CrN. Inclination of the TEM sample around the horizontal axis in plane with the layers confirmed that the multilayered structure was not destroyed by the plastic deformation and that there are not cracks in the multilayer coating that is contrary to other studies.[9] Calculated deformation (Table I) is in the range of ∼16% for NbN/CrN to 20% TiN/CrN of the initial coating thickness. The TiN/NbN combination [Fig. 9(b′)] did not show a multilayer rotation as deformation is mainly accommodated by shearing perpendicular to the film.

A detailed analysis of the multilayer deformation in the center of the indentation can be seen in Fig. 10. For indentation into a flat, elastic half space, there is a gradient in the stress intensity beneath the indenter such that the maximum stress is at the depth of roughly 50% of the contact radius below the surface. Therefore, it is not surprising that deformation of the multilayers is not homogeneous as a function of depth. A good example of this is seen in Fig. 10(c) for the NbN/CrN coating where the highest deformation is seen from layers 28 to 36 (first deposited layer is marked in Fig. 10 as a number 1) with relative compression reaching 50% for those periods. This cross section does provide some insight as to why the NbN/CrN film was characterized by sink-in for nanoscale indentations as seen with in situ movies. This could never be observed with any other method besides in situ SEM-indentation based technique since the final indent [Fig. 6(f)] shows a small amount of pileup. The plasticity of the CrN through most of the coating in Fig. 10(c) was confined by the stiffer NbN as a result of the crisp interfaces for these materials observed in Fig. 1. The flow in CrN and minimal deformation of NbN resulted in the formation of shear band extending for several layers [Fig. 9(f′)]. For example in Fig. 10(c),

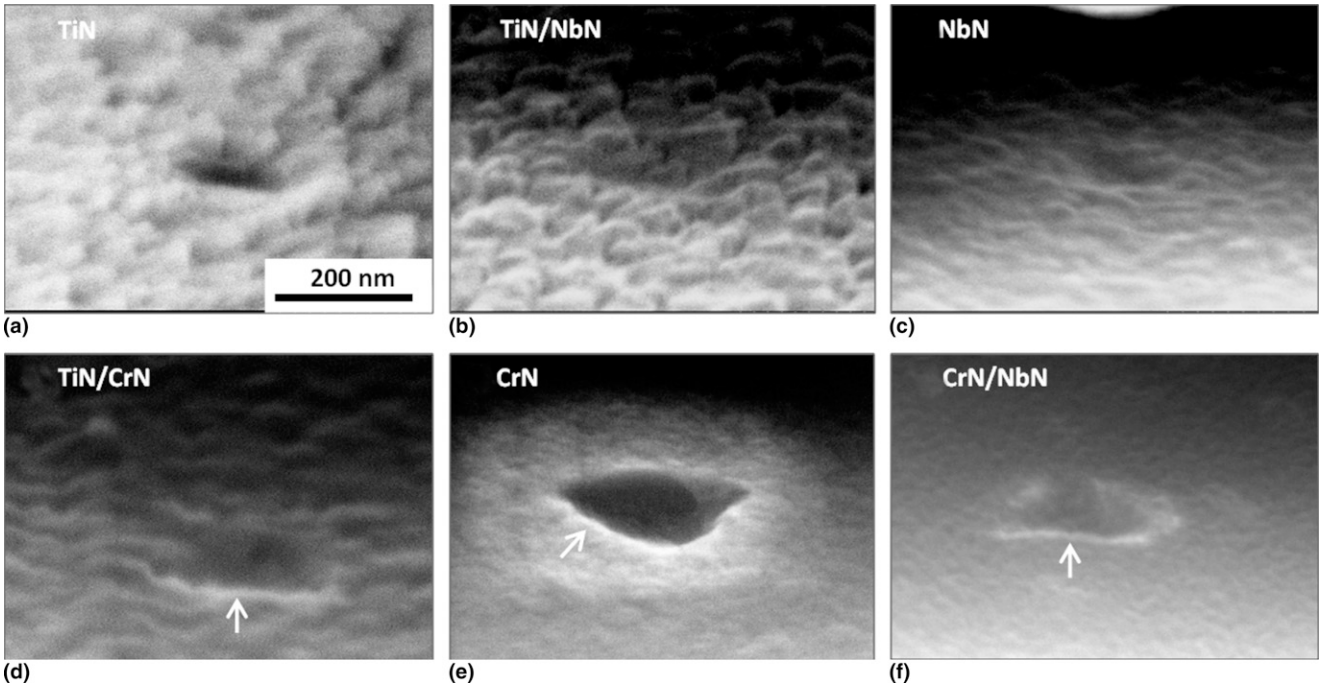

FIG. 6. In situ SEM nanoindentation images of the indentation imprints for a maximum load of 0.9 mN on the following coatings: (a) TiN, (b) TiN/NbN, (c) NbN, (d) TiN/CrN, (e) CrN, and (f) NbN/CrN.

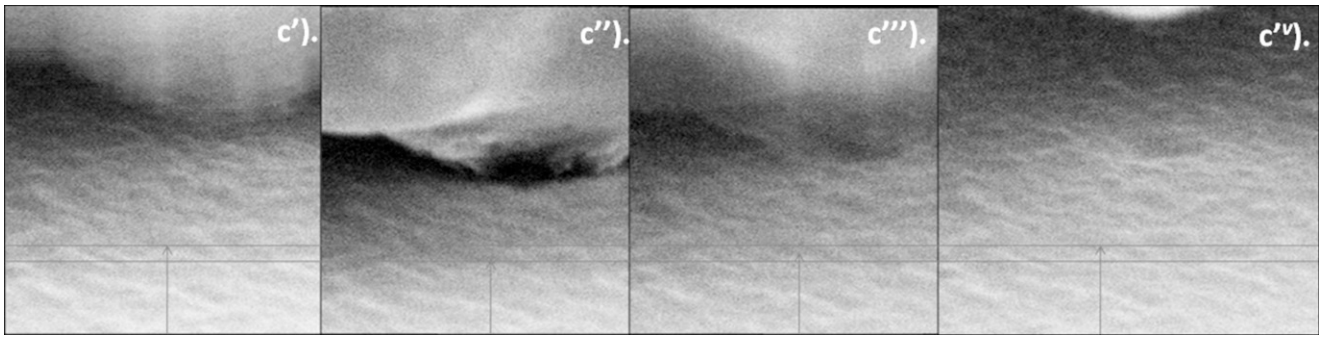

FIG. 7. Frames of the indentation from Fig. 6(c) showing sink-in of the NbN surface. (c′) Tip is approaching the sample surface. (c″) Maximum load (maximum sink-in may be observed). (c‴) Just after the tip retraction (sink-in did not recover fully yet). (c′ᵛ) Postmortem SEM image with full recovering of the sink-in phenomena.

TABLE II. Cracking measured for coatings during in situ micro-indentation for a maximum load of 150 mN.

Type of coating	Crack length for the max. load (μm)	Load for appearing of crack (mN)	Penetration depth (nm)
TiN	5.11	57	932
CrN	10.1	147	1771
NbN	...	...	...
TiN/NbN	9.8	73	1636
TiN/CrN	11.4	71.8	1440
NbN/CrN	3.8	133.4	652

the deformation of both constituent materials was approximately equal through layers 10 to 20 where stresses were lower than at layers 28 to 36 in this experiment. This similarity of deformation at larger indentation loads highlights the potential for nanolaminate strengthening at lower loads whereby a strong material and a tough material can combine their disparate properties into a single coating.

Uniformity of deformation is not seen in the other two multilayer combinations [Figs. 10(a) and 10(b)]. These materials possess rough interfaces and have grain orientations, which continue through multiple layers. For these films, strain localization was prevalent [Figs. 10(a) and 10(b)] and a rule-of-mixture with hardness (Table III) is found.

In the TiN/CrN substrate for 30 mN indentation, cracking in the substrate is generated during the loading part of the indentation experiment and can therefore be related to the pop-in in the load–displacement curve, as is discussed in Sec. III. D. Grain-boundary shearing for TiN is

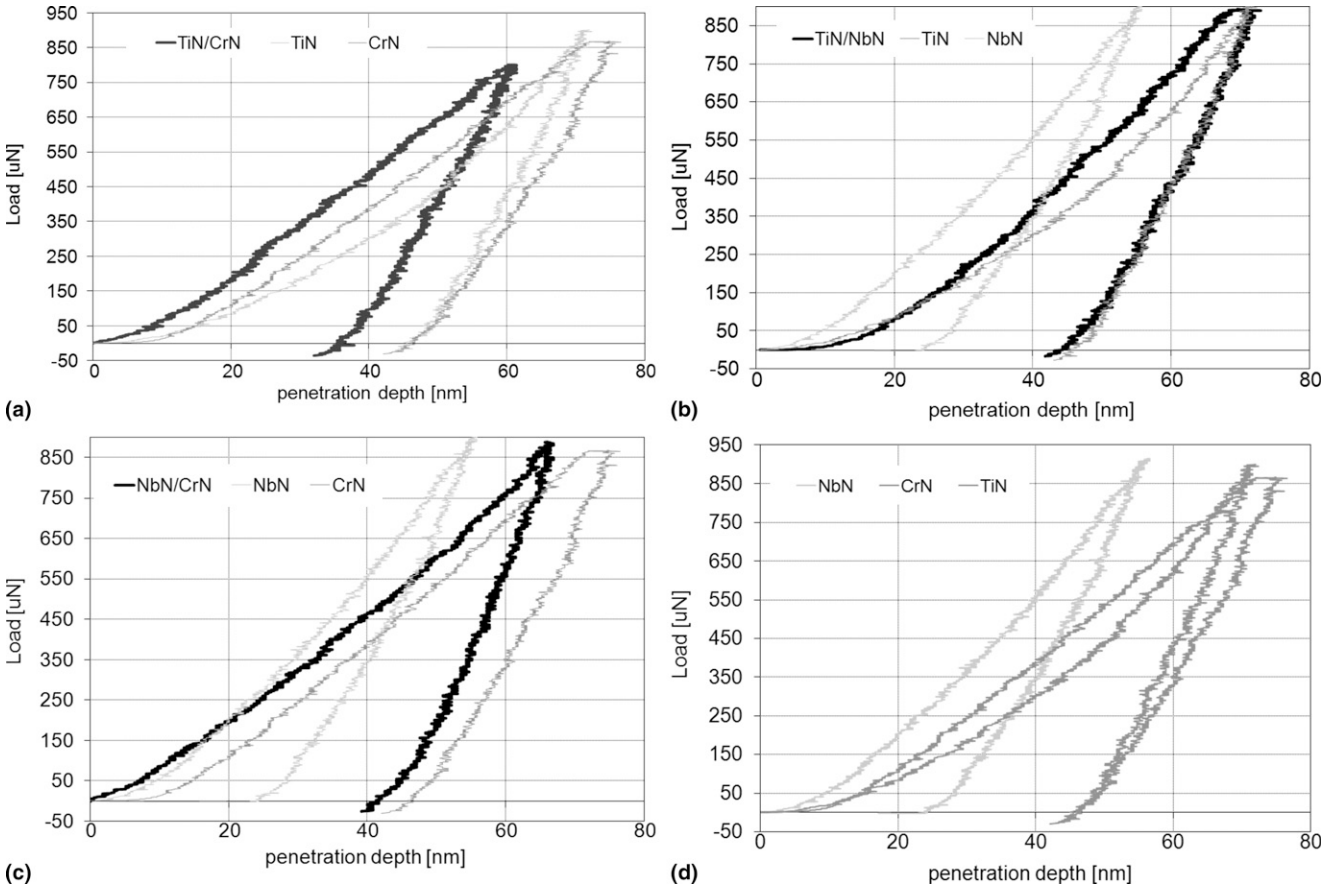

FIG. 8. Load–displacement curves recorded during in situ SEM nanoindentation presented in Fig. 6 for multilayers and corresponding reference coatings. (a) TiN/CrN, TiN and CrN. (b) TiN/NbN, TiN, and NbN. (c). NbN/CrN, NbN, and CrN. (d) TiN, CrN, and NbN. Surface roughness is evident as a lower slope at the initial stages (displacement < 20 nm) of the load–displacement curve.

TABLE III. Hardness values obtained by the Hysitron TriboIndenter and PicoIndenter

Type of coating	Hardness measured with TriboIndenter (GPa) 1000 μN	Hardness calculated from the in situ picoindentation (GPa) 850 μN
TiN	15.00	10.54
CrN	16.59	···
NbN	26.46	37.84
TiN/NbN	14.89	19.20
TiN/CrN	14.67	10.48
NbN/CrN	18.63	37.75

visible through shear steps at the substrate interface [Fig. 9(d′), arrow]. The TiN/NbN multilayer coating presents the most developed damage of the substrate where radial cracking is accompanied by symmetrical lateral cracks. Here, as seen in Fig. 9(b), the TiN sublayers deform to a larger extent than the NbN, which results in the through-thickness shearing of the NbN sublayers [Fig. 9(b′)]. Moreover, across the entire thickness of the multilayer coating, TiN layers exhibit a larger compression than NbN sublayers [Fig. 10(b)].

F. Overall deformation and fracture behavior

The combination of different measurement techniques, including in situ SEM micro- and nanoindentation, and cross-sectional TEM of the resulting deformation verified that the correlation of the appearance of cracks and discontinuities on the load–displacement curve is not always straightforward. In situ indentation has shown that many times cracks appear without a corresponding displacement burst. In fact, the cracking of the coatings is preceded by substrate cracking at lower loads for these coating/substrate combinations. All of the coatings, except NbN, show radial cracks having their source in the lateral substrate cracking. Even though the NbN did not crack, it did spall thus exposing the fracture that had occurred in the substrate as seen in the SEM micrograph of NbN [Fig. 3(c)]. The CrN reference coating plastically deforms starting with pileup, which develops into shear bands while the TiN deforms via grain-boundary sliding and cracking along the grain boundaries in addition to slight piling up and finally cracks.

The deformation mechanisms of the multilayers are characterized by the mechanisms of the constituent layers; however, they combine differently. For example,

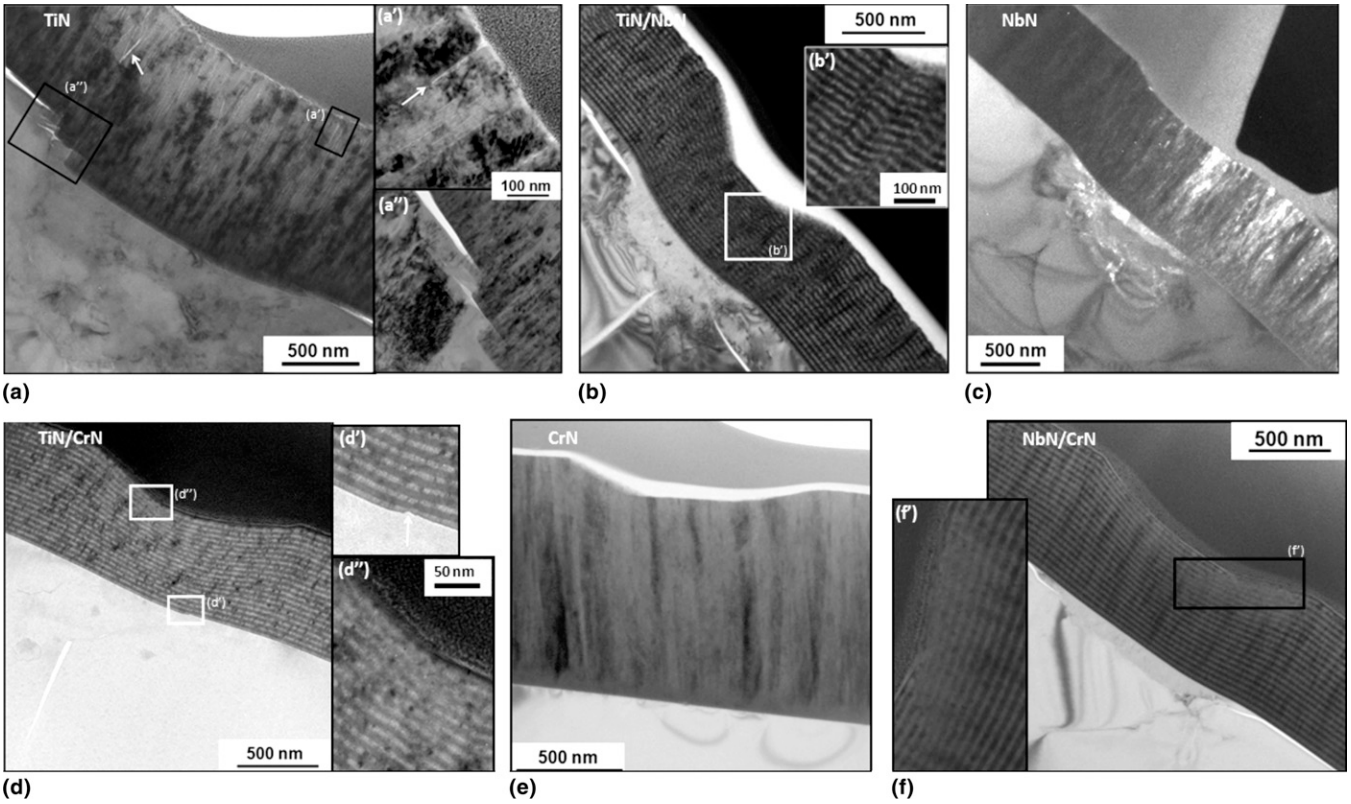

FIG. 9. TEM cross sections through indents (30 mN maximum load) performed on the coatings (a) TiN. (a′) Intergranular cracks. (a″) Shear steps at the surface/coating interface. (b) TiN/NbN. (b′) Showing grain-boundary sliding within TiN layers. (c) NbN. (d) TiN/CrN. (d′) Shear step caused by the TiN grain-boundary shearing at the coating/substrate interface. (d″) Layer rotation in the indentation imprint visible as a loss of sharpness. (e) CrN. (f) NbN/CrN. (f′) Showing shearing beneath the indentation imprint and layer rotation.

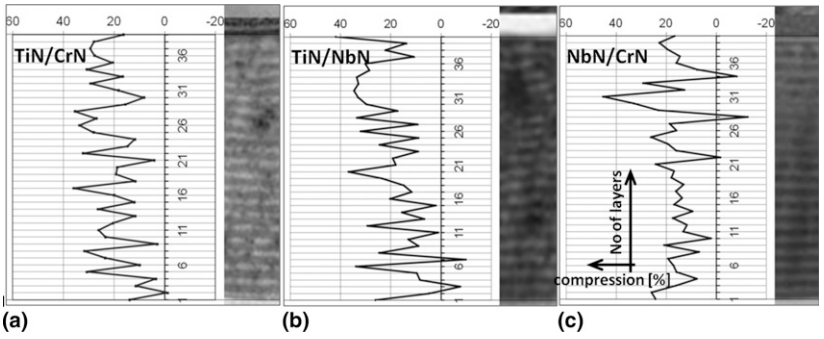

FIG. 10. Detailed analysis of the compression of the layers in the multilayer coatings through the thickness underneath the center of the 30 mN indents from Fig. 9 for: (a) TiN/CrN, (b) TiN/NbN, and (c) NbN/CrN.

grain-boundary sliding, which is characteristic for TiN, is much more apparent in the TiN/NbN combination, where NbN acts like a rigid plate, than for the TiN/CrN, where deformation is taken over by both constituent layers. Additionally, multilayers that contain NbN show improvement in adhesion compared with the NbN reference coating, and the pileup tendency of CrN is mitigated in the multilayer combinations. Qualitatively, larger deformation, longer cracks, and more pronounced fracture of the substrates underneath the indentation imprints was observed for the multilayers compared with the reference coatings.

At the nanoscale, each of the coatings exhibited specific mechanisms such as sink-in for NbN and NbN/CrN multilayers and varying degrees of pileup observed after unloading for CrN, TiN, TiN/CrN, and TiN/NbN. It should be noted that while the NbN/CrN coating shows minimal pileup after indentation, both it and the other coatings containing NbN exhibited sink-in behavior during indentation. Therefore, all coatings with NbN show an increase in hardness when calculating hardness from the in situ SEM images. The high nanohardness value (Table III) and smaller amount of compression (Table I) of the NbN/CrN combination relative to the

TiN/NbN coating was probably caused by the sharp and smooth interfaces that confine CrN plasticity. This is interesting since the TiN reference film deforms much less than the CrN reference film, and it shows that interfaces can play a significant role in overall deformation.

IV. CONCLUSIONS

Deformation and fracture mechanisms of the multilayer transition metal nitride coatings, TiN/CrN, TiN/NbN and NbN/CrN and corresponding reference coatings of TiN, NbN and CrN were systematically investigated using a combination of in situ micro- and nanoindentation and postmortem analysis of the indents by transmission electron microscopy. In situ SEM microindentation allowed for observation of fracture events, pileup, and sink-in of the coating/substrate system during indentation and demonstrated that fracture events do not always show up as discontinuities in the load–displacement curve. In situ SEM nanoindentation enabled the coating to be mechanically probed and roughness, pileup, and sink-in to be taken into account. In particular, the contact area calculated directly from the SEM image taken while the tip was under maximum load was shown to differ significantly from the one calculated using a standard Oliver and Pharr approach because of the factors mentioned previously. Postmortem TEM analysis of the deformed areas was used to assess the mechanisms of deformation of the coatings, and in particular an analysis of the compression ratio of the sublayers in the multilayers gave insight into the deformation mechanics at this scale.

Within measurement accuracy, the multilayer coatings exhibited no increase in hardness or reduced modulus when compared with the reference coatings. The deformation mechanisms of the multilayers are characterized by the mechanisms of the constituent layers; however, they do combine differently. Grain-boundary sliding, which is mechanism characteristic for TiN, is much more apparent in the TiN/NbN combination than in TiN/CrN. This is probably due to NbN-rigid-plate behavior in TiN/NbN, while in TiN/CrN the deformation is taken over by both constituent layers. Both multilayer coatings containing NbN exhibited sink-in during indentation; however, the NbN/CrN coating deforms less than the TiN/NbN combination, even though the reference films of CrN and TiN show the opposite behavior (Table I). It is thought that this is caused by the smooth interfaces that form in the NbN/CrN coating, compared with the TiN/NbN interfaces, such that the NbN is able to confine the CrN deformation. This example illustrates the importance of the state of the interface to the overall mechanical behavior of the coating and shows that the enhancement of constituent materials within a multilayer coating is possible.

ACKNOWLEDGMENTS

The authors would like to acknowledge S. Meier and J. Tharian, EMPA Duebendorf, for FIB samples preparation. We are grateful to Prof. R. Spolenak and M. Dietiker (ETH Zürich) for making the TriboIndenter accessible to our use and help in experiments. We thank Prof. W. Clegg and S. Corte (University of Cambridge) for helpful discussions. I also want to express special thanks to our colleagues form EMPA Thun, P. Schwaller, A. Bidiville, and F. Oestlund for fruitful discussions, M. Aeberhard for GDOES measurements, and G. Bürki for overall technical support. Finally, we acknowledge financial support from the European Commission in the framework of the project M3-2S under Contract No. 206486/1127.074.

REFERENCES

1. P.H. Mayrhofer, Ch. Mitterer, and L. Hultman: Microstructural design of hard coatings. *Prog. Mater. Sci.* **51,** 1032 (2006).
2. S.C. Tjong and H. Chen: Nanocrystalline materials and coatings. *Mater. Sci. Eng.* **45,** 1 (2004).
3. W.D. Sproul: New routes in preparation of mechanically hard films. *Science* **273,** 889 (1996).
4. I. Petrov, L. Hultman, U. Helmersson, J.E. Sundgren, and J.E. Green: Microstructure modification of TiN by ion bombardment during reactive sputter deposition. *Thin Solid Films* **169,** 299 (1989).
5. W.D. Sproul, P.J. Rudnik, and M.E. Graham: The effect of N_2 partial pressure, deposition rate and substrate bias potential on the hardness and texture of reactively sputtered TiN coatings. *Surf. Coat. Technol.* **39–40,** 355 (1989).
6. D.F. Arias, Y.C. Arango, and A. Devia: Study of TiN and ZrN thin films grown by cathodic arc technique. *Appl. Surf. Sci.* **253,** 1683 (2006).
7. Q. Yang, D.Y. Seo, and L.R. Zhao: Multilayered coatings with alternate pure Ti and TiNyCrN superlattice. *Surf. Coat. Technol.* **177–178,** 204 (2004).
8. B. Mirkarimi, S.A. Barnett, K.M. Hubbard, T.R. Jervis, and L. Hultman: Structure and mechanical properties of epitaxial $TiN/V_{0.3}Nb_{0.7}N$ (100) superlattices. *J. Mater. Res.* **9,** 1456 (1994).
9. C. Mendibide, J. Fontaine, P. Steyer, and C. Esnouf: Dry sliding wear model of nanometer scale multilayered TiN/CrN PVD hard coatings. *Tribol. Lett.* **17,** 779 (2004).
10. W.H. Zhang and J.H. Hsieh: Tribological behavior of TiN and CrN coatings sliding against an epoxy molding compound. *Surf. Coat. Technol.* **130,** 240 (2000).
11. M. Oden, C. Ericsson, G. Hakansson, and H. Ljungcrantz: Microstructure and mechanical behavior of arc-evaporated Cr–N coatings. *Surf. Coat. Technol.* **114,** 39 (1999).
12. G.A. Fontalvo, V. Terziyska, and C. Mitterer: High-temperature tribological behaviour of sputtered NbN_x thin films. *Surf. Coat. Technol.* **202,** 1017 (2002).
13. C.S. Sandu, M. Benkahoul, M. Parlinska-Wojtan, R. Sanjinés, and R. Lévy: Morphological, structural and mechanical properties of NbN thin films deposited by reactive magnetron sputtering. *Surf. Coat. Technol.* **200,** 6544 (2006).
14. Z. Han, X. Hu, J. Tian, G. Li, and G. Mingyuan: Magnetron sputtered NbN thin films and mechanical properties. *Surf. Coat. Technol.* **179,** 188 (2004).
15. Y.L. Su and J.S. Lin: An investigation of the tribological potential of TiN, CrN and TiN + CrN physical vapor deposited coatings in machine element applications. *Wear* **170,** 45 (1993).

16. Z.G. Zhang, O. Rapaud, N. Bonasso, D. Mercs, C. Dong, and C. Coddet: Control of microstructures and properties of dc magnetron sputtering deposited chromium nitride films. *Vacuum* **82,** 501 (2008).
17. I. Milosev, J.M. Abels, H-H. Strehblow, B. Naviasek, and M. Metikos-Hukovic: High temperature oxidation of thin CrN coatings deposited on steel. *J. Vac. Sci. Technol. A* **14,** 2527 (1996).
18. T. Hurkmans, D.B. Lewis, J.S. Brooks, and W-D. Munz: Chromium nitride coatings grown by unbalanced magnetron (UBM) and combined arc/unbalanced magnetron (ABS TM) deposition techniques. *Surf. Coat. Technol.* **86,** 192 (1996).
19. R. Hubler, A. Cozza, T.L. Marcondes, R.B. Souza, and F.F. Fiori: Wear and corrosion protection of 316-L femoral implants by deposition of thin films. *Surf. Coat. Technol.* **142,** 1078 (2001).
20. P. Panjan, B. Navinsek, A. Cvelbar, A. Zalar, and I. Milosev: Oxidation of TiN, ZrN, TiZrN, CrN, TiCrN, and TiN/CrN multilayer hard coatings reactively sputtered as a low temperature. *Thin Solid Films* **281,** 298 (1996).
21. S. Kanamori: Investigation of reactively sputtered TiN films for diffusion barriers. *Thin Solid Films* **136,** 195 (1986).
22. K. Hinode, Y. Homma, M. Horiuchi, and T. Takahashi: Morphology-dependent oxidation behavior of reactively sputtered titanium-nitride films. *J. Vac. Sci. Technol. A* **15,** 2017 (1997).
23. M.J. Deen: Effect of the deposition rate on the properties of d.c.-magnetron-sputtered niobium nitride thin films. *Thin Solid Films* **152,** 535 (1987).
24. D.F. Dawson-Elli, F. David, C.A. Fung, and J.E. Nordman: DC reactive magnetron sputtered NbN thin films prepared with and without hollow cathode enhancement. *IEEE Trans. Magn.* **27,** 1592 (1991).
25. I.L. Singer, R.N. Bolster, S.A. Wolf, E.F. Skelton, and R.A. Jeffries: Abrasion resistance, microhardness and microstructures of single-phase niobium nitride films. *Thin Solid Films* **107,** 207 (1983).
26. Y. Gotoh, M. Nagao, T. Ura, H. Tsuji, and J. Ishikawa: Ion-beam-assisted deposition of niobium nitride thin films for vacuum microelectronic devices. *Nucl. Instrum. Methods Phys. Res. B* **148,** 925 (1999).
27. K.S. Havey, J.S. Zabinski, and S.D. Walck: The chemistry, structure, and resulting wear properties of magnetron-sputtered NbN thin films. *Thin Solid Films* **303,** 238 (1997).
28. A. Mumtaz and W.H. Class: Color of titanium nitride prepared by reactive dc magnetron sputtering. *J. Vac. Sci. Technol.* **20,** 345 (1981).
29. B.J. Daniels, W.D. Nix, and B.M. Clemens: Enhanced mechanical hardness in compositionally modulated Fe(001)/Pt(001) and Fe(001)/Cr(001) epitaxial thin films. *Thin Solid Films* **253,** 218 (1994).
30. M. Nordin, M. Larsson, and S. Hogmark: Mechanical and tribological properties of multilayered PVD TiN/CrN,TiN/MoN, TiN/NbN and TiN/TaN coatings on cemented carbide. *Surf. Coat. Technol.* **106,** 234 (1998).
31. J.M. Molina-Aldareguia, S.J. Lloyd, S.J. Oden, T. Joelsson, L. Hultman, and W.J. Clegg: Deformation structures under indentations in TiN/NbN single-crystal multilayers deposited by magnetron sputtering at different bombarding ion energies. *Philos. Mag. A* **82,** 1983 (2002).
32. S.Y. Lee, G.S. Kim, and J.H. Hahn: Effect of the Cr content on the mechanical properties of nanostructured TiN/CrN coatings. *Surf. Coat. Technol.* **177,** 426 (2004).
33. H.C. Barshilia and K.S. Rajam: Structure and properties of reactive DC magnetron sputtered TiN/NbN hard superlattices. *Surf. Coat. Technol.* **183,** 174 (2004).
34. B.C. Kang, H.Y. Kim, O.Y. Kwon, and S.H. Hong: Bilayer thickness effects on nanoindentation behavior of Ag/Ni multilayers. *Scr. Mater.* **57,** 703 (2007).
35. M. Verdier, H. Huang, F. Spaepen, J.D. Embury, and H. Kung: Microstructure, indentation and work hardening of Cu/Ag multilayers. *Philos. Mag.* **86,** 5009 (2006).
36. Y-M. Luo, W. Pan, S.Q. Li, J. Chen, R.G. Wang, and J.Q. Li: Mechanical properties and microstructure of a Si_3N_4/Ti_3SiC_2 multilayer composite. *Ceram. Int.* **28,** 223 (2002).
37. V.I. Vdovin: Misfit dislocations in epitaxial heterostructures: Mechanisms of generation and multiplication. *Phys. Status Solidi A* **171,** 239 (1999).
38. J. Ding, Y. Meng, and S. Wen: Mechanical properties and fracture toughness of multilayer hard coatings using nanoindentation. *Thin Solid Films* **371,** 178 (2000).
39. N.J.M. Carvalho and J.Th.M. De Hosson: Deformation mechanisms in TiN/(Ti,Al)N multilayers under depth-sensing indentation. *Acta Mater.* **54,** 1857 (2006).
40. X. Chu and S.A. Barnett: Model of superlattice yield stress and hardness enhancements. *J. Appl. Phys.* **77,** 4403 (1994).
41. Y. Long, F. Giuliani, S.J. Lloyd, J. Molina-Aldareguia, Z.H. Barber, and W.J. Clegg: Deformation processes and the effects of microstructure in multilayered ceramics. *Composites: Part B* **37,** 542 (2006).
42. J. Musil, F. Kunc, H. Zeman, and H. Polakova: Relationships between hardness, Young's modulus and elastic recovery in hard nanocomposite coatings. *Surf. Coat. Technol.* **154,** 304 (2002).
43. H. Wrzesinska, P. Grabiec, Z. Rymuza, and M. Misiak: Influence of substrate on mechanical properties of TiN/NbN superlattices. *Microelectron. Eng.* **61,** 1009 (2002).
44. Y.L. Su and S.H. Yao: On the performance and application of CrN coating. *Wear* **205,** 112 (1997).
45. M. Okumiya and M. Griepentrog: Mechanical properties and tribological behavior of TiN-CrAlN and CrN–CrAlN multilayer coatings. *Surf. Coat. Technol.* **112,** 123 (1999).
46. O. Borrero-Lopez, M. Hoffman, A. Bendavid, and P.J. Martin: A simple nanoindentation-based methodology to assess the strength of brittle thin films. *Acta Mater.* **56,** 1633 (2008).
47. B. Moser, J.F. Löffler, and J. Michler: Discrete deformation in amorphous metals: An in situ SEM indentation study. *Philos. Mag.* **86,** 5715 (2006).
48. R. Rabe, J-M. Breguet, P. Schwaller, S. Stauss, F-J. Haug, J. Patscheider, and J. Michler: Observation of fracture and plastic deformation during indentation and scratching inside the scanning electron microscope. *Thin Solid Films* **469,** 206 (2004).
49. K.A. Rzepiejewska-Malyska, M. Parlinska-Wojtan, K. Wasmer, K. Hejduk, and J. Michler: In situ SEM indentation studies of the deformation mechanisms in TiN, CrN and TiN/CrN. *Micron.* **40,** 22 (2009).
50. H. Wrzesinska, J. Ratajczak, K. Studzinska, and J. Katcki: Transmission electron microscopy of hard ceramic superlattices applied in silicon micro-electro-mechanical systems. *Mater. Chem. Phys.* **81,** 265 (2003).
51. Y. Zhou, R. Asaki, W-H. Soe, R. Yamamoto, and R. Chen: Hardness anomaly, plastic deformation work and fretting wear properties of polycrystalline TiN/CrN multilayers. *Wear* **236,** 159 (1999).
52. J.R. Tuck, A.M. Korsunsky, D.G. Bhat, and S.J. Bull: Indentation hardness evaluation of cathodic arc deposited thin hard coatings. *Surf. Coat. Technol.* **139,** 63 (2001).
53. S. Veprek: The search for novel, superhard materials. *J. Vac. Sci. Technol. A* **17,** 2401 (1999).

54. H. Hollek: *Binary and Ternary Carbide and Nitride Systems of Transition Metals* (Gebrüder Borntraeger, Berlin, 1984).
55. K.A. Rzepiejewska-Malyska, R.C. Major, G. Buerki, E. Cyrankowski, S. Asif, O. Warren, and J. Michler: In situ mechanical observations during nanoindentation inside a high resolution scanning electron microscope. *J. Mater. Res.* **23,** 1973 (2008).
56. B. Naviasek, P. Panjan, and A. Cvelbar: Characterization of low temperature CrN and TiN (PVD) hard coatings. *Surf. Coat. Technol.* **74,** 155 (1995).
57. F. Hollstein, R. Wiedemann, and J. Scholz: Characteristics of PVD-coatings on AZ31hp magnesium alloys. *Surf. Coat. Technol.* **162,** 261 (2003).
58. W. Krysicki, J. Bartos, W. Dyczka, K. Królikowska, and M. Wasilewski: *The Theory of Probability and Mathematical Statistics in Exercises. Mathematical Statistics, Part 2* (Wydawnictwo Naukowe PWN, 2006).
59. V. Poulek, J. Musil, R. Cerny, and R. Kuzel: ε-Ti_2N phase growth control in titanium nitride films. *Thin Solid Films* **170,** L55 (1989).
60. P.R. LeClair: Titanium nitride thin films by the electron shower process. Ph.D. Thesis. Massachusetts Institute of Technology, Boston, MA (1998).
61. Yu.V. Levinskiy: Phase diagrams of metals with gases. *Russ. Metall.* **34,** (1974).
62. W. Lengauer, M. Bohn, B. Wollein, and K. Lisak: Phase reactions in the Nb–N system below 1400 C. *Acta Mater.* **48,** 2633 (2000).
63. M. Oden, U.J. Almer, G. Hakansson, and M. Olsson: Microstructure property relationships in arc-evaporated Cr–N coatings. *Thin Solid Films* **377,** 407 (2000).
64. C. Rebholz, H. Ziegele, A. Leyland, and A. Matthews: Structure, mechanical and tribological properties of nitrogen-containing chromium coatings prepared by reactive magnetron sputtering. *Surf. Coat. Technol.* **115,** 222 (1999).
65. W.C. Oliver and G.M. Pharr: An improved technique for determining hardness and elastic modulus using load and displacement sensing indentation experiments. *J. Mater. Res.* **7,** 1564 (1992).
66. S.J. Bull: Using work of indentation to predict erosion behavior in bulk materials and coatings. *J. Phys. D: Appl. Phys.* **39,** 1626 (2006).
67. A.M. Minor, E.A. Stach, J.W. Morris, and I. Petrov: In situ nanoindentation of epitaxial TiN/MgO (001) in a transmission electron microscope. *J. Electron. Mater.* **32,** 1023 (2003).